Mechanism of CDK5/p25 Binding by CDK Inhibitors

Marina Mapelli,[†] Lucia Massimiliano,[†] Claudia Crovace,[†,‡] Markus A. Seeliger,[§] Li-Huei Tsai,[||] Laurent Meijer,[⊥] and Andrea Musacchio*[,†]

Structural Biology Unit, Department of Experimental Oncology, European Institute of Oncology, Via Ripamonti 435, 20141 Milan, Italy, Department of Molecular and Cell Biology, Howard Hughes Medical Institute, University of California Berkeley, Berkeley, California 94720-3202, Department of Pathology, Harvard Medical School and Howard Hughes Medical Institute, 77 Avenue Louis Pasteur, Boston, Massachusetts 02115, and Cell Cycle Group, Station Biologique, B.P. 74, 29682 Roscoff Cedex, Bretagne, France

Received August 15, 2004

The cyclin-dependent kinases (CDK) CDK1, CDK2, CDK4, and CDK6 are serine/threonine protein kinases targeted in cancer therapy due to their role in cell cycle progression. The postmitotic CDK5 is involved in biological pathways important for neuronal migration and differentiation. CDK5 represents an attractive pharmacological target as its deregulation is implicated in various neurodegenerative diseases such as Alzheimer's, Parkinson's, and Niemann−Pick type C diseases, ischemia, and amyotrophic lateral sclerosis. We have generated an improved crystal form of CDK5 in complex with p25, a segment of the p35 neuronal activator. The crystals were used to solve the structure of CDK5/p25 with (*R*)-roscovitine and aloisine at a resolution of 2.2 and 2.3 Å, respectively. The structure of CDK5/p25/roscovitine provides a rationale for the preference of CDK5 for the R over the S stereoisomer. Furthermore, roscovitine stabilized an unusual collapsed conformation of the glycine-rich loop, an important site of CDK regulation, and we report an investigation of the effects of glycine-rich loop phosphorylation on roscovitine binding. The CDK5/p25 crystals represent a valuable new tool for the identification and optimization of selective CDK inhibitors.

Introduction

Cyclin-dependent kinase 5 (CDK5) is a member of a family of proline-directed serine/threonine kinases.[1] It regulates a variety of processes in developing and adult neurons.[2,3] CDK5 plays a central role in neuronal migration during the development of the central nervous system.[3] Mice lacking CDK5 or double deficient for its two brain activators p35 and p39 exhibit severe defects in the layering of the cerebral cortex.[4−6] CDK5 regulates the actin and microtubules cytoskeleton and modulates cell adhesion, neurite outgrowth, and cell motility.[2] More recently, many synaptic proteins have been shown to be CDK5 substrates, pointing to an involvement of CDK5 in various aspects of synaptic function, such as dopaminergic signaling, neurotransmitter release, and membrane cycling.[7,8]

p25 and p29 are equivalent proteolytic segments containing the C-terminal portion of p35 and p39, respectively. Excessive upregulation of CDK5 by the truncated activators contributes to neurodegeneration by altering the phosphorylation state of cytosolic and cytoskeletal proteins, and increased CDK5 activity has been implicated in Alzheimer's disease (AD), amyotrophic lateral sclerosis (ALS), Parkinson's disease, Niemann−Pick type C disease, and ischemia.[9−13] The mechanism of CDK5 activation by p25 has been recently clarified by the report of the crystal structure of the CDK5/p25 complex.[14] The classical dual mechanism of CDK activation consists of the binding of the cyclin box fold (CBF) region of the cyclins and the phosphorylation of the activation loop (also known as T-loop) by the CDK-activating kinase.[1,15,16] p25 contains a highly divergent CBF domain (Figure 1), which elicits an active conformation of CDK5 in the absence of phosphorylation.[14]

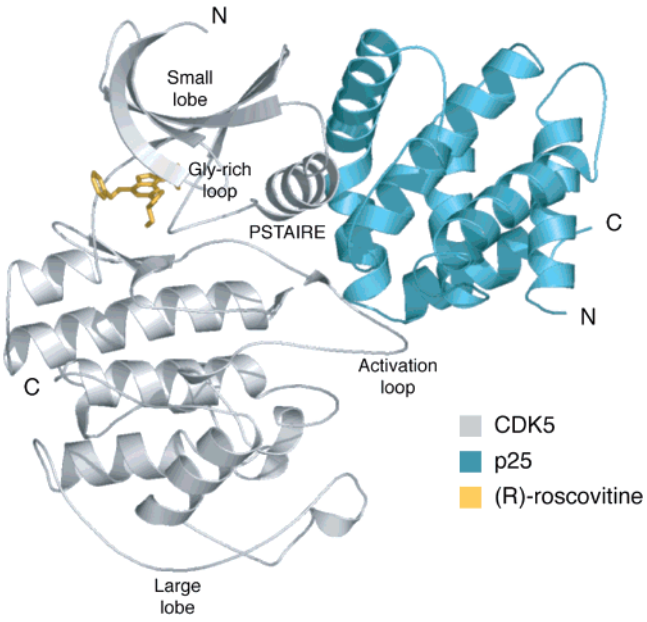

Figure 1. Ribbon diagram of the CDK5/p25 complex. CDK5 is shown in gray, p25 in blue. The ATP-binding pocket between the N and C terminal lobes of the kinase is occupied by (*R*)-roscovitine (yellow). The main structural elements of the kinase have been labeled.

* Corresponding author. Telephone: ++39 02 57489829. Fax: ++39 02 57489851. E-mail: andrea.musacchio@ifom-ieo-campus.it.
[†] European Institute of Oncology.
[‡] Present address: Medical Research Council (MRC) Laboratory of Molecular Biology, Hills Road, Cambridge CB2 2QH, U.K.
[§] University of California Berkeley.
[||] Harvard Medical School.
[⊥] Station Biologique.

10.1021/jm049323m CCC: $30.25
Published on Web 01/06/2005

Table 1. Data Collection and Refinement Statistics

	indirubin-3′-oxime	(*R*)-roscovitine	aloisine-A
	Data Collection		
space group	C2	$P3_221$	$P3_221$
beamline	ESRF ID14-1	ESRF ID14−2	ESRF ID14-2
unit cell dimensions (Å) and angles (deg)	$a = 149.54$ $b = 90.12$ $c = 83.16$ $\beta = 93.29$	$a = b = 117.99$ $c = 156.17$	$a = b = 117.72$ $c = 156.79$
resolution (Å)[a]	30.0−2.25 (2.3−2.25)	25.0−2.2 (2.3−2.2)	25.0−2.3 (2.4−2.3)
total observations	870805	570430	335266
unique reflections	50596	64818	53731
data completeness (%)	98.8 (99.9)	94.6 (97.7)	95.4 (97.5)
R_{sym} (%)[b]	7.5 (39.6)	11.3 (37.8)	10.4 (37.0)
$I/\sigma I$	20.4(4.5)	8.9 (2.8)	9.1 (2.6)
	Refinement		
resolution range (Å)	20.0−2.35	20.0−2.2	20.0−2.3
R_{conv}[c]/R_{free}[d]	22.8/25.7	21.3/24.4	21.3/25.2
number of protein atoms	6836	7098	6872
number of inhibitor atoms	42	26	40
number of solvent atoms	210	302	294
rmsd bond lengths (Å)	0.016	0.015	0.020
rmsd bond angles (deg)	2.0	1.4	1.8
mean B-factor protein (Å^2)	40.8	24.4	23.9
mean B-factor inhibitor (Å^2)	41.7	23.4	25.2

[a] Values in parentheses refer to the outer resolution shell. [b] $R_{symm} = \sum|I - \langle I\rangle|/\sum I$, where I is the observed intensity of a reflection and $\langle I\rangle$ is the average intensity obtained from multiple observations of symmetry-related reflections. [c] $R_{conv} = \sum||F_o| - |F_c||/\sum|F_o|$, where F_o and F_c are the observed and calculated structure factor amplitudes, respectively. [d] R_{free} is equivalent to R_{conv} for a 5% subset of reflections not used in the refinement.

Thus, CDK5 activation is clearly distinct from that of other cellular CDKs, which require phosphorylation of the activation loop for full activation.[1] Interestingly, a similar mechanism of CDK activation is also exploited by certain viral cyclins to highjack cellular CDKs, as revealed by the crystal structure of a CDK6/Vcyclin complex.[17] Another CBF-containing protein, known as Cables, binds CDK5 but does not seem to be able to activate its kinase activity.[18]

Deregulation of CDK5 is likely due to the release of CDK5/p25 from a membranous compartment, and subsequent hyperphosphorylation of substrates contributes to the disease state.[19] In particular, abnormal phosphorylation of the microtubule-binding protein Tau by deregulated CDK5 has been implicated in the formation of neurofibrillary tangles, a hallmark of AD.[10] In view of this role in pathogenesis, an increasing interest has developed in the search for CDK5 inhibitors.[20−23] A large body of structural knowledge on the inhibition of CDK family members as antitumor targets has developed in recent years using the CDK2 kinase as a model system.[24−26] Here, we report the identification of a new and improved crystal form of the CDK5/p25 kinase relative to the one that allowed the determination of the CDK5/p25 complex, which diffracted poorly.[14] The new crystal form introduces a new tool for the study of the structural bases of CDK/inhibitor interactions at high resolution, and we report the crystal structure of the active CDK5/p25 kinase complexed with the three inhibitor moieties (*R*)-roscovitine,[27−29] aloisine-A,[30] and indirubin-3′-oxime.[31] These chemical species are ATP antagonists binding into the well-conserved catalytic pocket of the kinase with IC_{50} values in the range of 0.1−0.2 μM. The structure with (*R*)-roscovitine (CYC202) is particularly interesting in view of the importance of this compound, which is now entering phase II clinical trials against cancer and phase I clinical tests against glomerulonephritis, following encouraging results obtained in preclinical tests.[29] The structures reveal the topology of the interactions between the inhibitors and the catalytic site, explain the preference of CDK5 for the (*R*)-roscovitine stereoisomer, and constitute a scaffold for structure-based drug design of more potent and selective inhibitors.

Results and Discussion

New Crystal Form. $CDK5^{D144N}$/p25 was initially crystallized in a monoclinic space group, and the structure was determined at 2.65 Å resolution.[14] We also used the monoclinic crystals for structure determination of the $CDK5^{D144N}$/p25/indirubin-3′-oxime complex, whose biological and modeling implications have been described recently.[32,33] However, the monoclinic crystals retained a platelike morphology, tended to grow in stacks, and were very fragile, making the handling required for intensive screening of inhibitors very laborious. We therefore attempted to grow a more robust crystal form. Primary seed stocks were prepared from the monoclinic crystals. These stocks were used to streak-seed preequilibrated drops. Seeding with the same seed stock yielded two different crystal forms depending on the composition of the drop. The original monoclinic crystal grew when the protein concentration ranged between 7 and 10 mg/mL or the PEG concentration was lower than 12% (w/v). At protein concentrations around 16 mg/mL and in the presence of 13−15% PEG 3350 and 0.1 M bis-Tris propane (pH 6.8−7.0), trigonal crystals grew instead. Repeated microseeding cycles performed with new seed stock generated by trigonal crystals reproducibly yielded new trigonal crystals of up to 0.4 × 0.2 × 0.2 mm^3 in size. Both lattices harbored two complexes in the asymmetric unit and proved suitable for diffraction experiments and derivatization with inhibitory compounds. The trigonal crystals (space group $P3_221$), however, were much more reproducible, were better diffracting, were more tolerant to DMSO (often required to solubilize hydrophobic compounds), and could be used to screen large batteries of inhibitors.

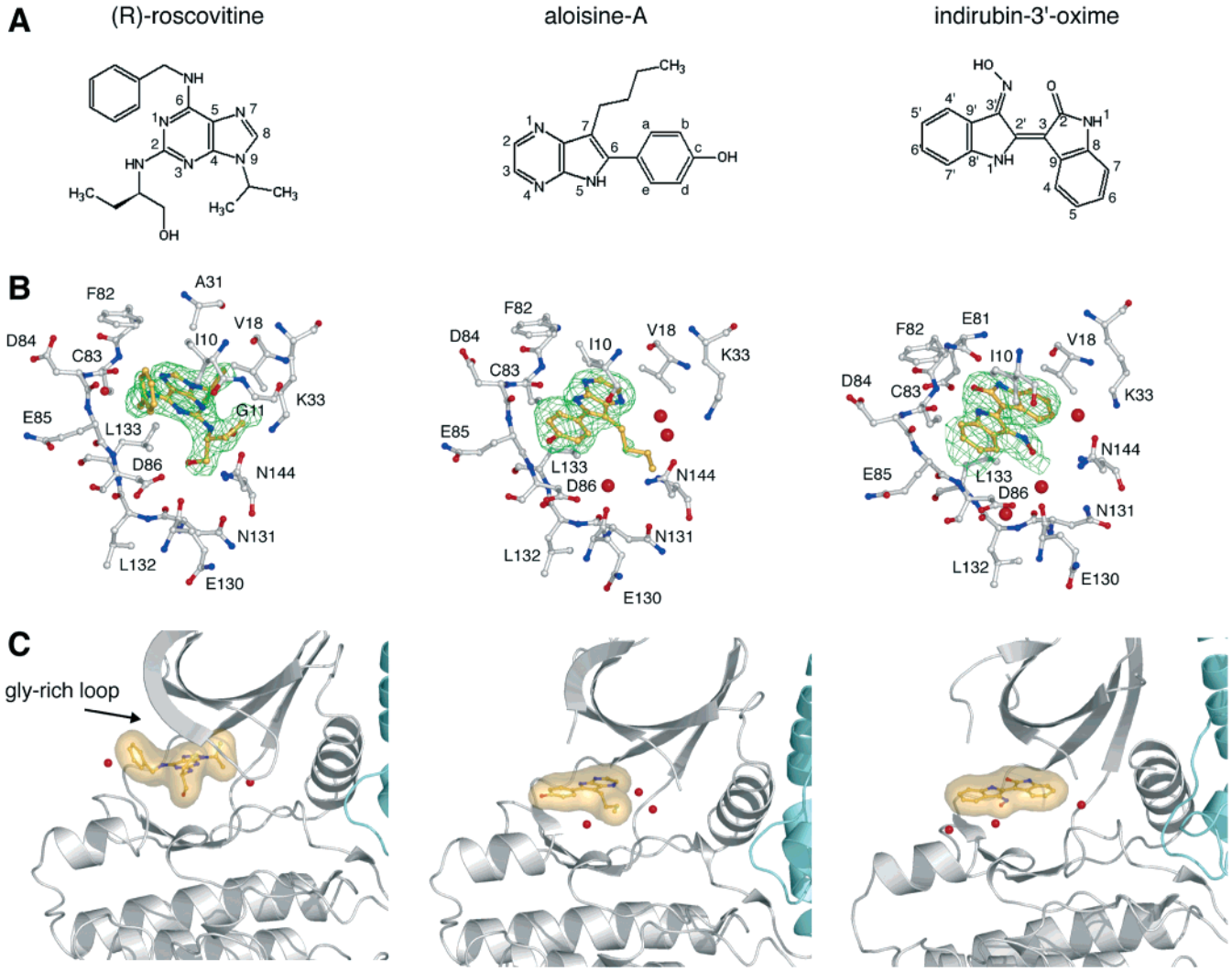

Figure 2. Mode of binding of (*R*)-roscovitine, aloisine-A, and indirubin-3′-oxime to CDK5/p25. (A) Structure of the inhibitors used in the crystallographic study. (B) Closeup of the catalytic site of the kinase. The residues of CDK5 that contact the bound ligands are depicted in ball-and-sticks, and the water molecules participating in hydrogen bonds are represented as red spheres. Carbon atoms are in gray (protein) and yellow (inhibitor), oxygen atoms are in red, and nitrogen atoms are in blue. Electron densities, calculated using ($|F_o| - |F_c|$) coefficients, are shown for the inhibitors only (contoured at 2σ level) and were computed using phases from models obtained at the end of the refinement with the inhibitor omitted. (C) Ribbon model of the CDK5/p25 complexes (same color code as in Figure 1) with a space-filling model of the inhibitors and of the waters in the nucleotide binding pocket (red spheres). Only the association of (*R*)-roscovitine induces the structuring of the glycine-rich loop, which is disordered in the other two structures.

We report the complexes of $CDK5^{D144N}$/p25 with (*R*)-roscovitine and aloisine-A as determined using the trigonal crystals. The structures were solved by molecular replacement and refined as described in Table 1.

Overall Conformation and Comparison of the Ligands in the Kinase Active Site. (*R*)-Roscovitine, aloisine-A, and indirubin-3′-oxime are planar substituted heterocyclic rings (Figure 2A), highly complementary to the ATP-binding cavity and deriving their affinity mainly by burial of the apolar side chains of the ATP-binding pocket as well as by formation of specific hydrogen bonds with the kinase (Figures 1 and 2). In CDK5, these concern the backbone carbonyl and the amide of Cys83, which act as hydrogen bond acceptor and donor, respectively (Figure 3B−D). This pattern of hydrogen bonding is also found in the complexes of CDK2 with several inhibitors, including among others purvalanol B, olomoucine, and roscovitine.[24,34−36] The orientation of the planar heterocyclic ring systems in the three CDK5−inhibitor complexes reported here is equivalent to those found for the equivalent compounds in complex with CDK2 (Figure 4).[35,37,38] Although the orientation of the heterocyclic ring is different in the three structures (Figure 3A and Figure 4), all three orientations are distinct from that of the adenine ring of ATP in the catalytic cleft of CDK2.[39]

CDK5/p25/Indirubin-3′-oxime. Indirubin is the key constituent of the traditional Chinese leukemia treatment Danggui Longhui Wan.[31] Indirubin-3′-oxime is also a potent inhibitor of CDK5/p25 ($IC_{50} = 0.10\ \mu M$) and GSK3-β ($IC_{50} = 0.022\ \mu M$).[40] The indirubin skeleton makes three direct hydrogen bonds with the backbone of the kinase; the NH group of Cys83 donates a hydrogen bond to the lactam amide oxygen, the cyclic nitrogen acts as a hydrogen bond donor to the backbone oxygen of Cys83, and the lactam amide nitrogen of the inhibitor donates a hydrogen bond to the peptide oxygen of Glu81 (Figure 3B). Moreover, the hydroxyl group of indirubin is indirectly hydrogen bonded to the side chain

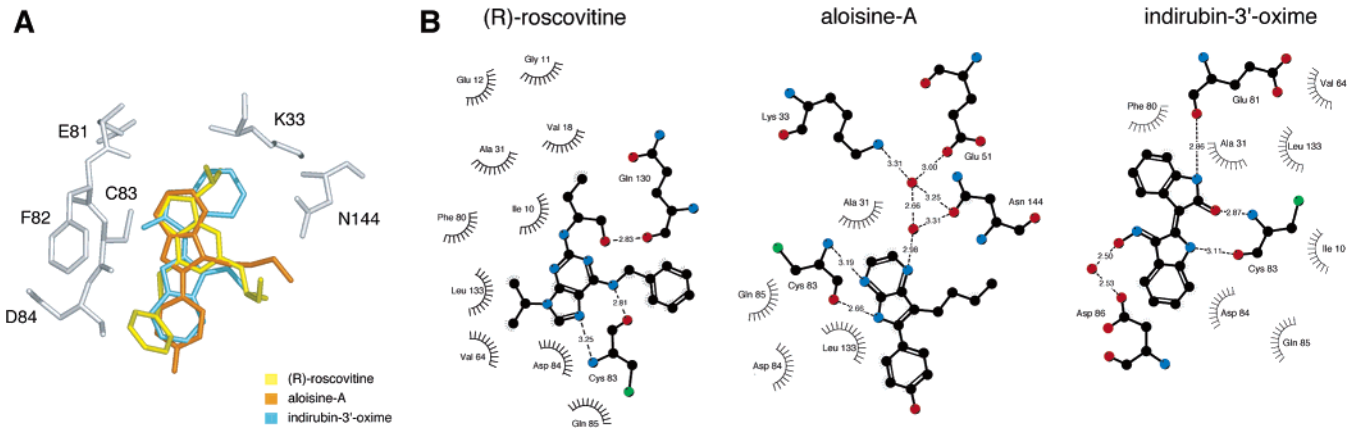

Figure 3. Analysis of contacts and orientation of the inhibitors. (A) The orientation of (*R*)-roscovitine (yellow), aloisine-A (orange), and indirubin-3′-oxime (blue) in the CDK5 active site after superposition of residues in the kinase small lobe. (B) Schematic drawing of CDK5 interaction with the inhibitors generated by LIGPLOT.[54] Residues forming van der Waals interactions are indicated as dashed moons, and those engaged in hydrogen bonds are shown as ball-and-stick drawings. Hydrogen bonds are depicted as dotted lines with the donor−acceptor distance given in angstroms.

of Asp86 via a bridging water molecule, and stacking interactions are made with Phe80.

CDK5/p25/Aloisine. Aloisine (6-phenyl[5H]pyrrolo-[2,3-*b*]pyrazines) scaffolds are selective inhibitors of CDK1/2/5 and GSK3-α/β.[30] Aloisine-A is most active on CDK5/p25 (IC_{50} = 0.16−0.20 μM). Aloisine-A carries a hydroxyl group at position C of the phenyl ring and a saturated alkyl chain $(CH2)_3-CH_3$ at position 7 (Figure 2A). In addition to the two hydrogen bonds between the nitrogen atoms N4 and N5 and the backbone amide and oxygen atoms of the Cys83, respectively, the nitrogen N1 is engaged in an hydrogen bonding network involving the side chains of Lys33, Glu51, Asn144, and two water molecules (Figure 3B). This bonding pattern targets the active state of the kinase, in which Lys33 and Glu51 are allowed to interact after rearrangement of the PSSALRE helix induced by p25 binding. The Asn144 rotamer is the one observed for Asp145 in apo-CDK2,[37] and it will need to be verified that the same hydrogen bond forms with wild-type CDK5/p25. The alkyl chain at position 7 is poorly visible in the electron density, indicating a high degree of flexibility and the existence of several conformations that can be accommodated in the groove normally hosting the ATP phosphate groups. The aloisine-A 4-hydroxyphenyl points out of the ATP binding cleft toward the surface of the CDK5 C-terminal domain, but the interaction in this region is suboptimal, as already described for the binding of aloisine-B to CDK2.[30] Larger substituents must be screened to exploit the interaction potential of this geometry. Being smaller than indirubin-3′-oxime and (*R*)-roscovitine, aloisine-A does not fill the back cleft of the ATP-binding pocket, resulting in reduced shape complementarity (Figure 2C).

CDK5/p25/(*R*)-Roscovitine. Roscovitine is a purine derivative (2-(1-ethyl-2-hydroxy-ethylamino)-6-benzylamino-9-isopropylpurine) containing an asymmetric carbon (Figure 2A). The R isomer displays higher CDK1 inhibitory activity than the S isomer.[35] In the CDK5/p25 complex, the oxygen of the chiral hydroxyethyl substituent of (*R*)-roscovitine is hydrogen bonded to the main chain carbonyl oxygen of Gln130, whereas the ethyl group is engaged in hydrophobic interactions with Ile10 and Val18 (Figure 3B). These contacts involve residues that are conserved between CDK1 and CDK5 and likely explain the preference of CDK1 for the R stereoisomer. Of note, the chiral C2 substituent of (*R*)-roscovitine in CDK5/p25 is rotated 182° around the N−C bond relative to what has been observed for the structure of (*R*)-roscovitine bound to CDK2 as well as the model of CDK5−roscovitine.[27,41]

Structures of apo-CDK2 complexed with (*R*)-roscovitine, aloisine-B, and indirubin-3′-oxime have been reported and show that the overall topology of binding is conserved between the two CDKs (Figure 4). Major differences in the interaction mode between the two kinases and the ligands have to be ascribed to the fact that CDK5/p25 is in the active conformation whereas apo-CDK2 is in an inactive status. CDK2 activity requires association with cyclin-A and phosphorylation of Thr160. Overall, this triggers a relative rotation of the N and C terminal lobes, repositioning of the PSTAIRE helix, and stretching of the activation loop.[1,15] The effects of these concerted motions on the geometry of the catalytic cleft can be summarized as (1) opening of the glycine-rich loop swinging away from the ATP-binding cavity toward the solvent, (2) inward movement of Glu51 of the PSTAIRE helix toward the ATP-binding cleft and subsequent formation of a water-mediated hydrogen-bonding network involving Lys33 and Glu51 and the side chain of Asp144, and (3) rearrangements of Phe80 and Phe82 as well as of the more distant His84 and Glu85.[37] As a result, only interactions taking place near the binding pocket for the adenine ring of ATP are preserved upon activation and are directly comparable (Figure 4).

Due to its flexibility, the glycine-rich loop of unliganded CDK5 is poorly visible in the electron density.[14] Although binding of aloisine-A and indirubin-3′-oxime do not affect the structure of the glycine-rich loop, (*R*)-roscovitine induces a restructuring of this mobile element, and excellent electron density is available for the entire segment (Figure 5A). Likely, this is due to the fact that Ile10, Gly11, and Glu12 in this loop participate in hydrophobic interactions with the inhibitor, reducing solvent access to the ATP-binding pocket. The large benzyl substituent protrudes into a hydrophobic pocket lined by Ile10 and Phe82 and extends into solvent.

Structuring of the glycine-rich loop also allows the visualization of the orientation of the CDK5 Tyr15 side

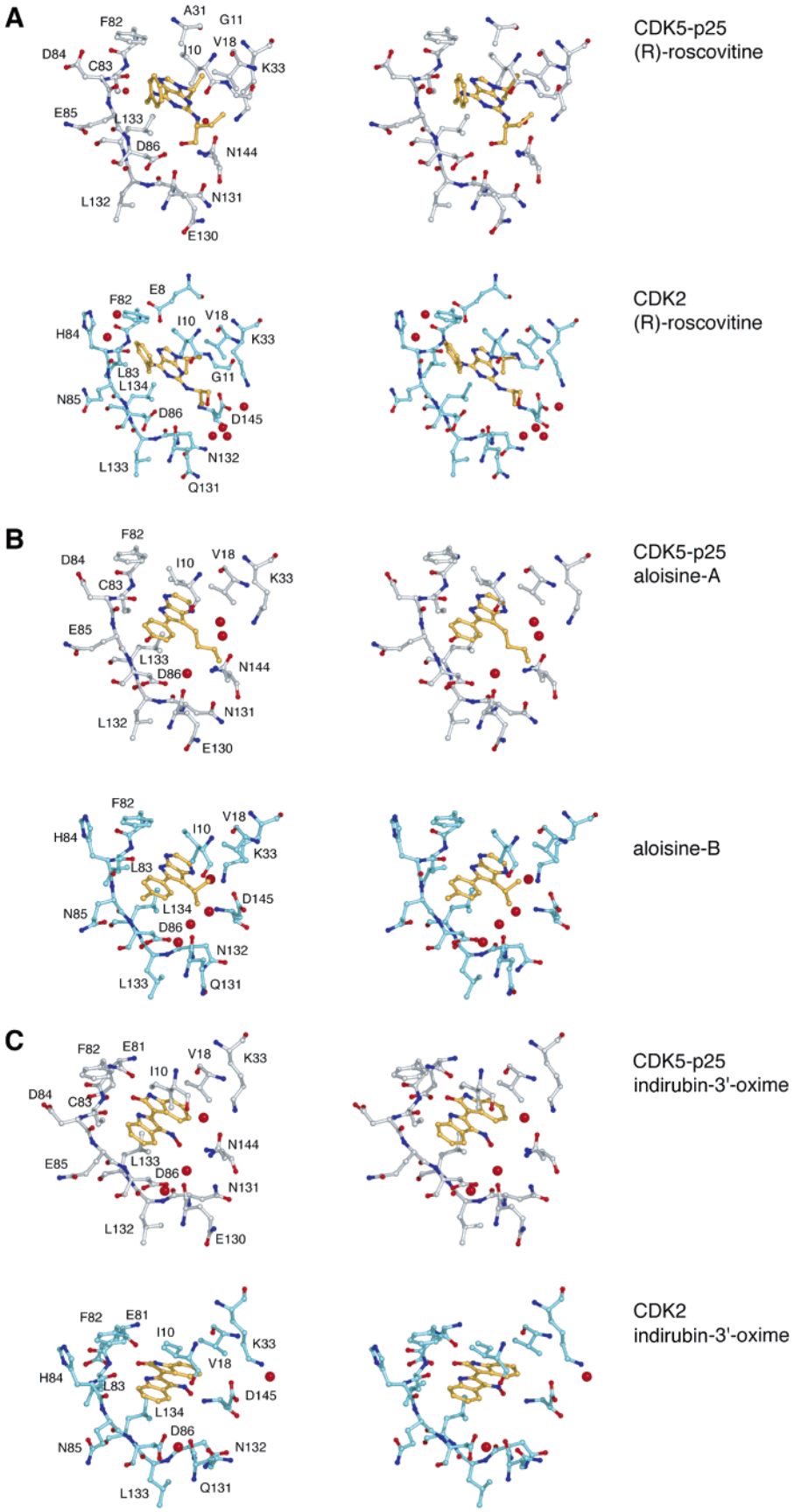

Figure 4. Comparison of CDK5 and CDK2 complexes with analogous compounds. Stereoviews of the nucleotide binding pocket of CDK5/p25 (gray) and apo-CDK2 (light blue) in complex with (A) (*R*)-roscovitine, (B) aloisine-A and -B. respectively, and (C) indirubin-3′-oxime. The residues and the water molecules involved in contacting the ligands are shown.

chain. It fits in the cleft between the catalytic site of the kinase and the PSSALRE helix, hydrogen bonding with Lys33 and Glu51 (Figure 5A). This position is essentially identical to that adopted by the equivalent

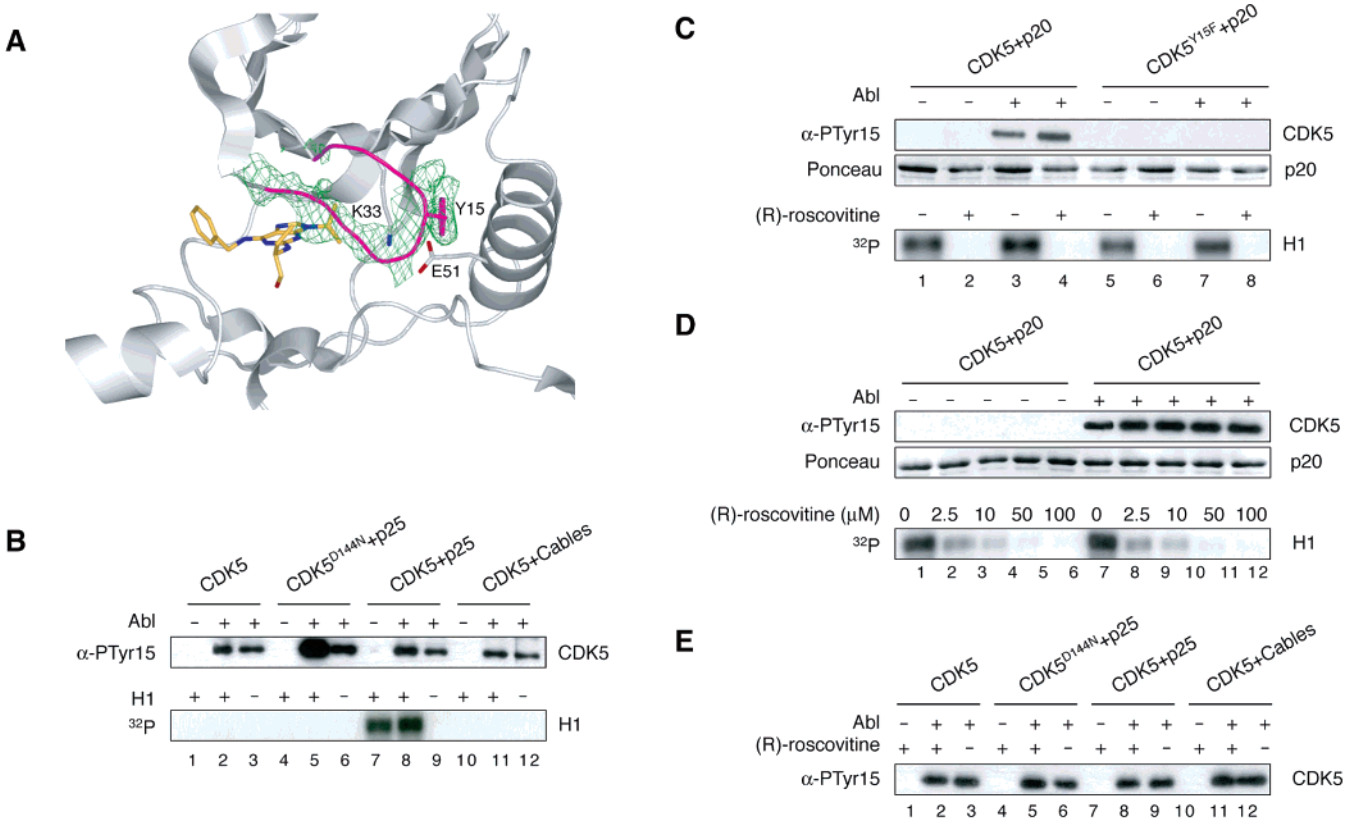

Figure 5. Structure and regulation of Tyr15 phosphorylation. (A) Effect of (*R*)-roscovitine binding on Tyr15 accessibility. Omit map of the glycine-rich loop of CDK5/p25 in complex with (*R*)-roscovitine contoured at 1.8σ level. The inhibitor and the side chains of Tyr15, Lys33, and Glu51 are represented as ball-and-sticks, and the glycine-rich loop is colored in magenta. The Tyr15 side chain is buried in the groove between the PSSALRE helix and the catalytic cleft. (B) Purified CDK5, alone or in complex with p25 and Cables$^{425-586}$, was used as a substrate of constitutively active Abl kinase, and the extent of phosphorylation was assessed by Western blot. The blot shows comparable phosphorylation levels for CDK5. Lower panel: Comparison of phosphorylated and unphosphorylated CDK5 activity on histone H1 assessed by ^{32}P incorporation. Only CDK5/p25 is active and shows modest upregulation upon Tyr15 phosphorylation. (C) CDK5^{wt} and CDK5^{Y15F} were incubated with Abl, and subsequently isolated using GST-p20 bound to solid phase. Upper panel: Only CDK5^{wt} was phosphorylated by Abl. Lower panel: kinase activity of the CDK5/GST-p20 complexes was evaluated on Histone H1 in the presence or absence of (*R*)-roscovitine. Kinase activity was inhibited in both cases. (D) The same experiment was repeated on CDK5^{wt} using growing concentrations of (*R*)-roscovitine. Histone H1 phosphorylation activity of Tyr15 phosphorylated or nonphosphorylated CDK5/p25 was equally sensitive to (*R*)-roscovitine. (E) CDK5 Tyr15 phosphorylation by Abl was assessed in the presence or absence of (*R*)-roscovitine and found to be identical.

CDK2 residue Tyr15 in the crystal structure of the ATP-bound CDK2/CyclinA complex containing unphosphorylated Thr160 (PDB ID code 1FIN). A similar position of Tyr15 is also observed in the structure of the ATP-bound CDK2/CyclinA complex after phosphorylation of Thr160 (PDB ID code 1JST). Remarkably, the side chain of Tyr15 flips out toward the substrate in the quaternary complex of phospho-Thr160-CDK2 with ATP, CyclinA, and a substrate peptide bound to the CDK2 active site (PDB ID code 1QMZ), possibly as a consequence of the realignment of the γ-phosphate of ATP upon substrate binding.[39,42,43] Most likely, this flipped conformation of Tyr15 is also the one adopted by this residue after phosphorylation, one of the key regulatory switches impinging on CDKs.[44] The presence of a phosphate group on the side chain of Tyr15 would almost certainly prevent its burial into the small lobe as described above for our structure of CDK5/p25 with (*R*)-roscovitine and for CDK2 structures 1FIN and 1JST. However, a flipped and fully exposed conformation of the side chain as observed in the 1QMZ dataset is much more likely also to represent the conformation of Tyr15 after its phosphorylation. An interesting possible implication of these observations for our studies of the CDK5/p25 complex with *R*-roscovitine is that a phoshporylated Tyr15 (phospho-Tyr15) might be expected to be incompatible with the collapsed conformation of the glycine-rich loop observed in our crystal structure of CDK5/p25/roscovitine, suggesting that phospho-Tyr15-CDK5 might escape inhibition by roscovitine or be a poorer substrate. To test this, we assessed whether previous phosphorylation of Tyr15 by Abl would decrease the potency of (*R*)-roscovitine inhibition of CDK5. Initially, we looked at the ability of Abl to phosphorylate CDK5 and how CDK5 activity was affected by Tyr15 phosphorylation (Figure 5B). Apo-CDK5, CDK5^{D144N}/p25, CDK5^{wt}/p25, and CDK5/Cables were exposed to Abl. After 1 h, Gleevec was added to inhibit the Abl kinase, and a fraction of the samples was analyzed by Western blotting (WB) using an antibody against phosphorylated Tyr15. All of the samples were effectively phosphorylated in an Abl-dependent fashion. This shows that at least in vitro CDK5 does not require interacting with Cables to be phosphorylated on Tyr15, as suggested previously.[18] The remaining part of the reaction was added to histone H1, and CDK5 activity was evaluated (Figure 5B). Only the CDK5^{wt}/p25 complex was found to be active. In agreement with previous reports,[18,45] Tyr15 phosphorylation

produced a small but reproducible increase in CDK5 activity (lanes 7 and 8). This is a distinctive difference between CDK5 and other CDK family members, which are usually inhibited after phosphorylation of Tyr15.[44]

To evaluate the effects of (*R*)-roscovitine on differently phosphorylated forms of CDK5, recombinant Abl was added to $CDK5^{wt}$ or $CDK5^{Y15F}$ in a phosphorylation reaction, after which CDK5 and Abl were separated using GST-p20 bound to a solid phase (p20 is a segment of p25/p35 that contains the minimal CDK5 binding and activation domain). An antibody was used to detect phosporylated Tyr15 by Western blot (Figure 5C, upper panel). This confirmed that Abl phosphorylates CDK5 on Tyr15 (Figure 5C, lanes 3 and 4). The CDK5 samples were then used in a histone H1 kinase assay to test the effect of Tyr15 phosphorylation on CDK5 activity and the sensitivity to (*R*)-roscovitine of the differently phosphorylated forms of CDK5. As above, Tyr15 phosphorylation caused a small increase in the activity of CDK5 (lanes 1 and 3). (*R*)-Roscovitine, however, appeared to be equally effective in inhibiting the activity of the different isoforms (lanes 2 and 4). This shows that CDK5 will not escape inhibition by (*R*)-roscovitine when phosphorylated. To corroborate these data, we repeated the experiment using increasing concentrations of (*R*)-roscovitine (Figure 5D). In both cases, we observed complete inhibition of CDK5 at (*R*)-roscovitine concentrations in the range 10−50 μM.

Because unphosphorylated Tyr15 is buried within the small lobe of CDK5 after binding of (*R*)-roscovitine, we also considered the possibility that the addition of (*R*)-roscovitine depressed Tyr15 phosphorylation by Abl. To test this, apo-CDK5, $CDK5^{D144N}$/p25, $CDK5^{wt}$/p25, and CDK5/Cables were exposed to Abl in the presence or absence of (*R*)-roscovitine, and the degree of Tyr15 phosphorylation was evaluated by Western blot. In all cases, the presence of (*R*)-roscovitine did not significantly alter the degree of phosphorylation of Tyr15.

Conclusions

We report a new versatile protocol to characterize the structure of ATP-competitive inhibitors bound to the CDK5/p25 active site. In particular, we have obtained a very well diffracting crystal form of this complex, consistently providing X-ray diffraction data to high resolution. This new tool represents a very useful addition to crystals of CDK2 and of the CDK2/cyclinA complex, which to our knowledge have until now been the sole tool to address the mode of binding of CDK inhibitors to the CDK active site. The CDK5/p25 crystals might provide an alternative to the CDK2 crystals for all those inhibitors whose cocrystallization with CDK2 proved impossible due to specific technical limitations. Furthermore, the collection of large datasets of crystallographic models of small molecule inhibitors bound into the active site of different members of the CDK family may eventually provide useful information on structural differences that should be exploited for the design of selective inhibitors. Finally, the availability of crystals of CDK5/p25, together with pure and active kinase for in vitro studies, is particularly important to understand specific aspects of the regulation of CDK5, a protein whose deregulation is implicated in several neurodegenerative disorders (Introduction) and that represent a drug target of its own.

The importance of this approach is evidenced by our study of the interaction of the CDK5/p25 complex with (*R*)-roscovitine. Besides providing a model of this inhibitor in the CDK5 active site for comparison with previously reported structures of (*R*)-roscovitine bound to CDK2,[35,37] we also provided an answer to the question whether CDK5 previously phosphorylated on Tyr15 displayed different susceptibility to inhibition by (*R*)-roscovitine relative to the unphosphorylated counterpart, an issue specifically arising from our structure that has not been investigated before in detail. Our data allow concluding that the phosphorylation of Tyr15, a step that activates CDK5, does not render the CDK5/p25 complex any less susceptible to inhibition by (*R*)-roscovitine.

This result offers a further piece of evidence for the extraordinary plasticity of protein kinases. It also suggests the possibility that the conformational space explored by the kinase may be exploited for the development of drugs targeting selectively certain conformations (and therefore activation states) of the kinase. These may include conformations specifically induced by other protein ligands, such as p35, p39, or Cables in the case of CDK5. The best illustration of this principle is the binding of Gleevec to the active site of Abl.[46] In the complex of Gleevec with Abl, the inhibitor forces the activation loop into an inactive conformation, in which the conserved DFG motif at the entry of this loop is diverted from its usual conformation, so that the phenylalanine points into the ATP-binding site and the aspartate will no longer coordinate the magnesium. The inhibitors described in this study, roscovitine, aloisine, and indirubin, are significantly smaller than Gleevec and are unable to span the distance to the activation segment. As a consequence, this segment (and the DFG motif in particular) does not change its structure in the presence of these inhibitors relative to the uninhibited structure. Future studies on CDK inhibitors will have to address the possibilities offered by the new concepts, and we feel confident that the tools described in this report will prove useful toward this end.

Experimental Section

Data Collection, Structure Determination and Refinement. For crystallization, we used a $CDK5^{D144N}$/p25 kinase dead mutant, as this provides better expression yields relative to the wild-type complex.[14] This mutant complex was produced by infecting cells with a single dual recombinant baculovirus and purified as described.[14] Crystallization of p25/CDK5 was carried out by the hanging drop vapor diffusion technique using the streak-seeding method for crystal optimization. The original monoclinic crystals were used to generate stocks of seeds for microseeding. Primary seed stocks were prepared by transferring a small crystal to 2 μL of reservoir solution and by crushing it with a sharp tip. This stock was serially diluted to 1:10, 1:100, and 1:300 and used to streak-seed drops preequilibrated for about 16 h (see text for more details). For inhibitor soaking, the crystals were harvested into a stabilizing solution of 13% (w/v) PEG 3350, 100 mM KI, 100 mM bisTris−propane (pH 7), and 10 mM DTT supplemented with 1 μL of 10−100 mM inhibitor molecule previously dissolved in DMSO. The maximum DMSO concentration tolerated by the crystals in these soaks was around 4%. Soaks were carried out for 48−72 h, and crystals were subsequently cryoprotected by stepwise addition of stabilizing solution plus 50% (w/v) glycerol up to a final concentration of 20% glycerol before freezing in liquid nitrogen. Data were collected at beamlines ID14-1 and ID14-2 of the European Synchrotron

Radiation Facility (ESRF) on an ADSC Q4R detector ($\lambda = 0.933$ Å). Data processing and reduction were carried out with the HKL package.[47] Details of the data collection and reduction are reported in Table 1. The structure was determined by molecular replacement with the atomic coordinates of the CDK5/p25 complex (Protein Data Bank code 1H4L) as the search model utilizing the program AMORE.[48] Already after the first cycles of rigid-body refinement, difference Fourier maps displayed clear electron densities in the active site for all the three inhibitors. At this stage, a run of 15 cycles of ARP/wARP[49] was performed to improve the density in the active site without model bias. The resulting density was used to manually fit the inhibitor models whose geometry was generated with the DRG program.[50] Subsequent refinement was pursued with alternating cycles of interactive model building and CNS[51] or REFMAC[52] program suites. Bulk solvent correction and anisotropic B-factor scaling were applied throughout the refinement procedures. Toward the end of the refinement, waters were added using the water-pick routine included in CNS. TLS refinement was implemented at the end of the refinement protocol to separately model the anisotropic movement of the N- and C-terminal lobes of CDK5 and of p25. In the case of the trigonal crystals, the electron density map was significantly weaker for one of the two CDK5/p25 complexes contained in the asymmetric unit, and all the analysis here reported relies on the complex displaying the best electron density. The final model of the complex with (*R*)-roscovitine consists of residues 1−292 for CDK5 and 145−293 for p25, whereas in the complexes with alosine-A and indirubin-3′-oxime the glycine-rich loop of CDK5 (residues 11−14) is not visible. In the complex with indirubin-3′-oxime also, the residues 39−42 of CDK5 are unstructured, and two further residues at the N-terminus of p25 are not visible. Final refinement statistics are reported in Table 1. Coordinates of CDK5/p25 in complex with (*R*)-roscovitine, aloisine-A, and indirubin-3′-oxime are available from the Protein Data Bank with the ID codes 1UNL, 1UNG and 1UNH, respectively.

Production of Active Wild-Type CDK5/p25 and Abl. The cDNA encoding wild-type CDK5 was subcloned into the pFastBac 1 transfer vector (GIBCL-BRL), and the baculovirus expression vector was generated according to the manufacture's guidelines. The active CDK5/p25 complex was produced as follows. Suspension cultures of Sf9 were grown to a density of 10^6 cells/mL at 27 °C and infected with the CDK5 and p25 baculoviruses at a ratio experimentally defined to provide similar expression levels of each subunit. Cells were harvested 72 hpi and washed in a phophate-buffered saline solution. Pelleted Sf9 cells were resuspended in a buffer containing 40 mM Tris-HCl (pH 8), 0.2 M NaCl, 2 mM β-mercaptoethanol, 1 mM PMSF, and a tablet of a protease inhibitor cocktail (Roche). Cells were lysed by sonication, and the extracts were clarified by centrifugation at 150000 *g* for 45 min at 4 °C. The supernatant was applied to a 5-mL HiTrap metal chelating column (Pharmacia) loaded with $NiCl_2$ and equilibrated in the same buffer used for lysis. The column was washed in the equilibration buffer supplemented with 20 mM imidazole, and the complex eluted with a linear gradient from 20 to 200 mM imidazole in 15 column volumes. The peak fractions corresponding to the complex were pooled and loaded onto a Sephadex G-25 desalting column (Pharmacia) to adjust the buffer to 10 mM Tris (pH 8), 0.2 M NaCl, 5% glycerol, 1 mm EDTA, and 5 mM DTT and subsequently concentrated in a stirred ultrafiltration cell (Amicon) prior to application on a Superdex 75 sizing column. The strategy yields approximately 1 mg of pure protein from 1 L of suspension culture. An analogous protocol was employed to produce the complex of CDK5 with a fragment of human Cables encompassing residues 425−568 where a putative cyclin-box fold is located.[18]

Murine Abelson (Abl) kinase domain (residues 227−512) was cloned into pET28a (Novagen) as a fusion with a TEV cleavable N-terminal hexahistidine tag. Transformed BL21 DE3 cells were grown to an OD (600 nm) of 1.2 and induced with 1 mM IPTG at 20 °C for 16 h. Cells were harvested, resuspended in 50 mM Tris pH 8.0, 250 mM NaCl, and 1 mM DTT, and lysed by sonication. Insoluble material was pelleted by centrifugation (20 min, 40 000*g*), and the insoluble pellet containing the Abl kinase domain was resuspended in 8 M urea, 50 mM Tris pH 8.0, and 1 mM DTT. Protein was refolded in 50 mM Tris pH 7.7, 1 mM DTT, 10 mM $MgCl_2$, and 400 mM Sucrose and purified by ion exchange and size exclusion chromatography. Activity of the refolded material was monitored by the coupled kinase assay as described before.[53]

Phosphorylation of CDK5 on Tyr15 and in Vitro Kinase Assays. Kinase reactions were assembled in a final volume of 30 μL and contained 0.2−1 μg of CDK5 in 40 mM HEPES/KOH (pH 8), 40 μM K/glutamate, 8 mM $MgCl_2$, 1 mM EGDA, 0.5 mM EDTA, 2 mM DTT, 0.1−0.02 mM ATP, and 0.25 mM $NaVO_4$, and the desired concentration of constitutively active Abl. When required, (*R*)-roscovitine was added up to a final concentration of 200 μM. The mixtures were incubated for 1 h at 30 °C, and the phosphorylation levels were assessed by Western blot analysis using anti phospho-Tyr15-CDC2 antibodies (Cell Signaling). To compare the kinase activity of phosphorylated and unphosphorylated CDK5, GST-p20 preabsorbed on GSH beads was added to the mixtures and incubated for 15 min, after which the newly formed GST-p20/CDK5 complexes were washed with kinase buffer devoid of Abl. When Tyr15 phoshorylation was carried out on preformed CDK5/p25 or CDK5/Cables complexes, Abl activity was inhibited by addition of Gleevec to the mixture together with ^{32}P-γATP and histone H1. Half of this sample was used to assess the state of Tyr15 phosphorylation by Western blot, whereas the other half was supplemented with 5 γCi of ^{32}P-γATP, 1 μg of histone H1, and the indicated amounts of (*R*)-roscovitine in order to compare the kinase activity of phoshporylated and unphosphorylated CDK5. The reaction was incubated for 1 h at 30 °C, subsequently resolved on a 14% acrylamide−bisacrylamide SDS gel, and incorporation of ^{32}P was visualized by autoradiography.

Acknowledgment. We thank the Alzheimer's Association and the Telethon Foundation for generous funding. M.M. is a postdoctoral fellow of the Italian Foundation for Cancer Research. A.M. is a scholar of the Italian Foundation for Cancer Research and an EMBO Young Investigator. Thanks to John Kuriyan and his laboratory for support and helpful discussions.

References

(1) Mapelli, M.; Musacchio, A. The structural perspective on CDK5. *Neurosignals* **2003**, *12*, 164−172.
(2) Dhavan, R.; Tsai, L. H. A decade of CDK5. *Nat. Rev. Mol. Cell. Biol.* **2001**, *2*, 749−759.
(3) Gupta, A.; Tsai, L. H. Cyclin-dependent kinase 5 and neuronal migration in the neocortex. *Neurosignals* **2003**, *12*, 173−179.
(4) Ohshima, T.; Ward, J. M.; Huh, C. G.; Longenecker, G.; Veeranna; et al. Targeted disruption of the cyclin-dependent kinase 5 gene results in abnormal corticogenesis, neuronal pathology and perinatal death. *Proc. Natl. Acad. Sci., U.S.A.* **1996**, *93*, 11173−11178.
(5) Gilmore, E. C.; Ohshima, T.; Goffinet, A. M.; Kulkarni, A. B.; Herrup, K. Cyclin-dependent kinase 5-deficient mice demonstrate novel developmental arrest in cerebral cortex. *J. Neurosci.* **1998**, *18*, 6370−6377.
(6) Ko, J.; Humbert, S.; Bronson, R. T.; Takahashi, S.; Kulkarni, A. B.; et al. p35 and p39 are essential for cdk5 function during neurodevelopment. *J. Neurosci.* **2001**, *21*, 6758−6671.
(7) Cheng, K.; Ip, N. Y. Cdk5: A new player at synapses. *Neurosignals* **2003**, *12*, 180−190.
(8) Bibb, J. A. Role of cdk5 in neuronal signaling, plasticity, and drug abuse. *Neurosignals* **2003**, *12*, 191−199.
(9) Nguyen, M. D.; Julien, J. P. Cyclin-dependent kinase 5 in amyotrophic lateral sclerosis. *Neurosignals* **2003**, *12*, 215−220.
(10) Lau, L. F.; Ahlijanian, M. K. Role of CDK5 in the pathogenesis of Alzheimer's disease. *Neurosignals* **2003**, *12*, 209−214.
(11) Smith, P. D.; Crocker, S. J.; Jackson-Lewis, V.; Jordan-Sciutto, K. L.; Hayley, S.; et al. Cyclin-dependent kinase 5 is a mediator of dopaminergic neuron loss in a mouse model of Parkinson's disease. *Proc. Natl. Acad. Sci., U.S.A.* **2003**, *100*, 13650−13655.
(12) Bu, B.; Li, J.; Davies, P.; Vincent, I. Deregulation of CDK5, hyperphosphorylation, and cytoskeletal pathology in the Niemann−Pick type C murine model. *J. Neurosci.* **2002**, *22*, 6515−6525.

(13) Wang, J.; Liu, S.; Fu, Y.; Wang, J. H.; Lu, Y. CDK5 activation induces hippocampal CA1 cell death by directly phosphorylating NMDA receptors. *Nat. Neurosci.* **2003**, *6*, 1039−1047.
(14) Tarricone, C.; Dhavan, R.; Peng, J.; Areces, L. B.; Tsai, L.; et al. Structure and regulation of the CDK5−p25(nck5a) complex. *Mol. Cell* **2001**, *8*, 657−669.
(15) Pavletich, N. P. Mechanisms of cyclin-dependent kinase regulation: structures of CDKs, their cyclin activators, and Cip and INK4 inhibitors. *J. Mol. Biol.* **1999**, *287*, 821−828.
(16) Hisanaga, S.; Saito, T. The regulation of cyclin-dependent kinase 5 activity through the metabolism of p35 or p39 CDK5 activator. *Neurosignals* **2003**, *12*, 221−229.
(17) Schulze-Gahmen, U.; Kim, S. H. Structural basis for CDK6 activation by a virus-encoded cyclin. *Nat. Struct. Biol.* **2002**, *9*, 177−181.
(18) Zukerberg, L. R.; Patrick, G. N.; Nikolic, M.; Humbert, S.; Wu, C. L.; et al. Cables links CDK5 and c-Abl and facilitates CDK5 tyrosine phosphorylation, kinase upregulation, and neurite outgrowth. *Neuron.* **2000**, *26*, 633−646.
(19) Patrick, G. N.; Zukerberg, L.; Nikolic, M.; de la Monte, S.; Dikkes, P.; et al. Conversion of p35 to p25 deregulates CDK5 activity and promotes neurodegeneration. *Nature* **1999**, *402*, 615−622.
(20) Lau, L. F.; Seymour, P. A.; Sanner, M. A.; Schachter, J. B. CDK5 as a drug target for the treatment of Alzheimer's disease. *J. Mol. Neurosci.* **2002**, *19*, 267−273.
(21) Sausville, E. A. Complexities in the development of cyclin-dependent kinase inhibitor drugs. *Trends. Mol. Med.* **2002**, *8*, S32−37.
(22) Fischer, L.; Endicott, J.; Meijer, L. Cyclin-dependent kinase inhibitors. In *Cell Cycle Regulators as Therapeutic Targets*; Meijer, L., Je'ze'quel, A., Roberge, M., Eds.; CNRS, Station Biologique de Roscoff: Roscoff, France, 2003; pp 235−248.
(23) Knockaert, M.; Greengard, P.; Meijer, L. Pharmacological inhibitors of cyclin-dependent kinases. *Trends Pharmacol. Sci.* **2002**, *23*, 417−425.
(24) Fischer, P. M.; Endicott, J.; Meijer, L. Cyclin-dependent kinase inhibitors. *Prog. Cell Cycle Res.* **2003**, *5*, 235−248.
(25) Furet, P. X-ray crystallographic studies of CDK2, a basis for cyclin-dependent kinase inhibitor design in anti-cancer drug research. *Curr. Med. Chem. Anti. Canc. Agents* **2003**, *3*, 15−23.
(26) Davies, T. G.; Pratt, D. J.; Endicott, J. A.; Johnson, L. N.; Noble, M. E. Structure-based design of cyclin-dependent kinase inhibitors. *Pharmacol. Ther.* **2002**, *93*, 125−133.
(27) De Azevedo, W. F.; Leclerc, S.; Meijer, L.; Havlicek, L.; Strnad, M.; et al. Inhibition of cyclin-dependent kinases by purine analogues: Crystal structure of human CDK2 complexed with roscovitine. *Eur. J. Biochem.* **1997**, *243*, 518−526.
(28) Meijer, L.; Kim, S. H. Chemical inhibitors of cyclin-dependent kinases. *Methods Enzymol.* **1997**, *283*, 113−128.
(29) Meijer, L.; Raymond, E. Roscovitine and other purines as kinase inhibitors. From starfish oocytes to clinical trials. *Acc. Chem. Res.* **2003**, *36*, 417−425.
(30) Mettey, Y.; Gompel, M.; Thomas, V.; Garnier, M.; Leost, M.; et al. Aloisines, a new family of CDK/GSK-3 inhibitors. SAR study, crystal structure in complex with CDK2, enzyme selectivity, and cellular effects. *J. Med. Chem.* **2003**, *46*, 222−236.
(31) Hoessel, R.; Leclerc, S.; Endicott, J. A.; Nobel, M. E.; Lawrie, A.; et al. Indirubin, the active constituent of a Chinese antileukaemia medicine, inhibits cyclin-dependent kinases. *Nat. Cell Biol.* **1999**, *1*, 60−67.
(32) Meijer, L.; Skaltsounis, A. L.; Magiatis, P.; Polychronopoulos, P.; Knockaert, M.; et al. GSK-3-selective inhibitors derived from Tyrian purple indirubins. *Chem. Biol.* **2003**, *10*, 1255−1266.
(33) Polychronopoulos, P.; Magiatis, P.; Skaltsounis, A. L.; Myrianthopoulos, V.; Mikros, E.; et al. Structural basis for the synthesis of indirubins as potent and selective inhibitors of glycogen synthase kinase-3 and cyclin-dependent kinases. *J. Med. Chem.* **2004**, *47*, 935−946.
(34) Schulze-Gahmen, U.; Brandsen, J.; Jones, H. D.; Morgan, D. O.; Meijer, L.; et al. Multiple modes of ligand recognition: Crystal structures of cyclin-dependent protein kinase 2 in complex with ATP and two inhibitors, olomoucine and isopentenyladenine. *Proteins* **1995**, *22*, 378−391.
(35) De Azevedo, W. F.; Leclerc, S.; Meijer, L.; Havlicek, L.; Strnad, M.; et al. Inhibition of cyclin-dependent kinases by purine analogues: Crystal structure of human cdk2 complexed with roscovitine. *Eur. J. Biochem.* **1997**, *243*, 518−526.
(36) Gray, N. S.; Wodicka, L.; Thunnissen, A. M.; Norman, T. C.; Kwon, S.; et al. Exploiting chemical libraries, structure, and genomics in the search for kinase inhibitors. *Science* **1998**, *281*, 533−538.
(37) Davies, T. G.; Tunnah, P.; Meijer, L.; Marko, D.; Eisenbrand, G.; et al. Inhibitor binding to active and inactive CDK2: The crystal structure of CDK2−cyclin A/indirubin-5-sulphonate. *Structure* **2001**, *9*, 389−397.
(38) Mettey, Y.; Gompel, M.; Thomas, V.; Garnier, M.; Leost, M.; et al. Aloisines, a new family of CDK/GSK-3 inhibitors. SAR study, crystal structure in complex with CDK2, enzyme selectivity, and cellular effects. *J. Med. Chem.* **2003**, *46*, 222−236.
(39) Brown, N. R.; Noble, M. E.; Endicott, J. A.; Johnson, L. N. The structural basis for specificity of substrate and recruitment peptides for cyclin-dependent kinases. *Nat. Cell Biol.* **1999**, *1*, 438−443.
(40) Leclerc, S.; Garnier, M.; Hoessel, R.; Marko, D.; Bibb, J. A.; et al. Indirubins inhibit glycogen synthase kinase-3 beta and CDK5/p25, two protein kinases involved in abnormal tau phosphorylation in Alzheimer's disease. A property common to most cyclin-dependent kinase inhibitors? *J. Biol. Chem.* **2001**, *276*, 251−260.
(41) Filgueira de Azevedo, W., Jr.; Gaspar, R. T.; Canduri, F.; Camera, J. C., Jr.; Freitas da Silveira, N. J. Molecular model of cyclin-dependent kinase 5 complexed with roscovitine. *Biochem. Biophys. Res. Commun.* **2002**, *297*, 1154−1158.
(42) Russo, A. A.; Jeffrey, P. D.; Pavletich, N. P. Structural basis of cyclin-dependent kinase activation by phosphorylation. *Nat. Struct. Biol.* **1996**, *3*, 696−700.
(43) Jeffrey, P. D.; Russo, A. A.; Polyak, K.; Gibbs, E.; Hurwitz, J.; et al. Mechanism of CDK activation revealed by the structure of a cyclinA-CDK2 complex. *Nature* **1995**, *376*, 313−320.
(44) Morgan, D. O. Principles of CDK regulation. *Nature* **1995**, *374*, 131−134.
(45) Sasaki, Y.; Cheng, C.; Uchida, Y.; Nakajima, O.; Ohshima, T.; et al. Fyn and CDK5 mediate semaphorin-3A signaling, which is involved in regulation of dendrite orientation in cerebral cortex. *Neuron* **2002**, *35*, 907−920.
(46) Schindler, T.; Bornmann, W.; Pellicena, P.; Miller, W. T.; Clarkson, B.; et al. Structural mechanism for STI-571 inhibition of abelson tyrosine kinase. *Science* **2000**, *289*, 1938−1942.
(47) Otwinowski, Z.; Minor, W. Processing of X-ray diffraction data collected in oscillation mode. In *Macromolecular Crystallography, Part A*; Academic Press: New York, 1997; pp 307−326.
(48) Navaza, J. Implementation of molecular replacement in AMoRe. *Acta Crystallogr, Sect. D: Biol. Crystallogr.* **2001**, *57*, 1367−1372.
(49) Lamzin, V. S.; Wilson, K. S. Automated Refinement for Protein Crystallography. *Macromolecular Crystallography*; Academic Press: New York, 1997; pp 269−305.
(50) van Aalten, D. M. F.; Bywater, R.; Findlay, J. B. C.; Hendlich, M.; Hooft, R. W. W.; et al. PRODRG, a program for generating molecular topologies and unique molecular descriptors from coordinates of small molecules. *J. Comput.-Aided Mol. Des.* **1996**, *10*, 255−262.
(51) Brunger, A. T.; Adams, P. D.; Clore, G. M.; DeLano, W. L.; Gros, P.; et al. Crystallography & NMR system: A new software suite for macromolecular structure determination. *Acta Crystallogr., Sect. D: Biol. Crystallogr.* **1998**, *54*, 905−921.
(52) Collaborative Computational Project, N. The CCP4 suite: Programs for protein crystallography. *Acta Crystallogr., Sect. D: Biol. Crystallogr.* **1994**, *50*, 760−763.
(53) Schindler, T.; Bornmann, W.; Pellicena, P.; Miller, W. T.; Clarkson, B.; et al. Structural mechanism for STI-571 inhibition of abelson tyrosine kinase. *Science* **2000**, *289*, 1938−1942.
(54) Wallace, A.; Laskowski, R.; Thornton, J. LIGPLOT: A program to generate schematic diagrams of protein−ligand interactions. *Protein Eng.* **1995**, *8*, 127−134.

JM049323M